Chapter 5

Collective transport of interacting vesicles on microtubules

5.1 Introduction

In the last chapter, we saw how various transport properties related to bidirectional movement of cargo vesicles and organelles can be calculated within a simple, single-particle model. However at high concentration of transport vesicles, of relevance in *in-vivo* situations, one cannot ignore inter-vesicle interactions. Indeed measurements of mitochondrial distribution and movement in cultured neurons show that [1],

1. the distribution of mitochondria in actively growing axons is highly skewed towards the growth cone, with a seven fold higher density in the region immediately adjacent to the growth cone than in a region 100 μm away.

2. for such growing axons, the percentage of *motile* mitochondria, was three times higher in those further from the growth cone than in the ones that were nearer.

Taken together, these observations highlight the importance of inter-organelle interaction, either direct or indirect (via cytoskeletal remodeling). Further, it reveals the limitations of the simple, single-particle model for vesicle transport, as it cannot provide information about the spatial distribution of cargo vesicles. The effect of finite boundaries on the spatial distribution of cargo vesicles can be significant as they are loaded and off-loaded at specific locations on the microtubule [2, 3, 4]. Including the effects of interactions and therefore spatial variation in the model described in Chapter 4, would give rise to a host of possible steady states and a complex phase diagram, which can be analysed using Monte-Carlo simulation. We will leave this elaborate exercise to later.

We will instead, focus on a simple *minimal* model for collective transport, incorporating interactions between the vesicles and effects due of finite boundary, which will address more generic statistical mechanics issues related to steady states and phases in non-equilibrium driven transport [5, 6, 7]. This minimal model belongs to a class of transport models which have been used to study a diverse range of phenomenon such as vehicular traffic on roads [8, 9], driven granular gases [7, 10] and motor transport [11]. Such driven systems are characterized by novel non-equilibrium steady states [6, 7, 12, 13] and boundary induced phase transitions [11, 15, 16]. We believe that such an approach could provide the conceptual underpinnings for a more general model of vesicle transport.

A particular example of driven transport models is the so called Totally Asymmetric Exclusion Process (TASEP), originally proposed in [17]. In this model, the ‘particles’ hop unidirectionally with a single rate and interact via hard-core repulsion. The interplay between

conservation of particle number in the bulk and the rate of incoming and outgoing particles at the boundaries, drives the system to nontrivial steady state [18]. The phase diagram shows continuous and discontinuous transitions of the average density of particles, even in the limit of large system sizes [19]. This is to be contrasted with systems in thermal equilibrium, where the boundary conditions do not affect bulk behaviour, when the system size is large enough. These results have been obtained by a combination of exact techniques [21, 22], Monte Carlo simulations [15], mean-field method and domain wall analysis [15].

In a similar spirit, we will introduce a minimal model for the dynamics of vesicles carried by two species of processive motors. By analysing the dynamics and its steady states, we will find a phase diagram, determined by boundary conditions and inter-conversion.

After introducing the minimal 4-species model for bidirectional transport (Section 5.2) of different motor-vesicle complexes (called 'species'), we look at the limit of 'fast' inter-conversion rate among the various species (Section 5.3). In Section 5.4, we analyse the mean-field dynamics in the continuum limit and obtain the corresponding steady state solutions. In Section 5.5, we briefly review the nature of steady states of TASEP in terms of domain wall dynamics. We use this approach in our steady state analysis, the nature of the phases and phase boundaries of our minimal model. We compare these results with Monte-Carlo simulations and find exact agreement for the density and current profile in the bulk. We illustrate the diverse nature of phases obtained by varying entry rates, exit rates and inter-conversion rates. In Section 5.6, we discuss the 'fast' inter-conversion limit in the context of vesicular transport on microtubules and possible extensions of the current work.

5.2 A minimal model for bidirectional transport: 4-species model

Recall that in Chapter 4, the state of the moving cargo vesicle, $|n, m\rangle$, was entirely described by n attached dyenin and m attached kinesin motors. The maximum allowed values of n and m were N and M respectively. In the minimal model, we will restrict the maximum number of attached dyenin and kinesin to 1. We will however include the effects of interaction via excluded volume and the effects of finite boundaries on the collective vesicular transport.

We define a vesicle with kinesin attached to the microtubule filament as (+), a vesicle with dyenin attached to the filament as (−), a vesicle with both dyenin and kinesin attached to filament as (±), and a vacancy (absence of vesicle) as (0). These consitute the 4 'species' in our minimal model. Then we look at directed motion of the motor-vesicle complex along

the 1-dimensional microtubule track. It is convenient to start with a lattice description and take the continuum limit.

The (+) and (−) hop, on the lattice with the same rates but opposite direction if and only if the adjacent hopping site is vacant. Thus (+) species hop to the right and (−) species hop to the left, with rate 1. The (±) species do not hop at all. However (±) can be transformed to (+) or (−), with forward and backward rates of conversion. This is to be understood as a change of state of the vesicle due to the stochastic attachment and detachment of the motor to the cellular filament track (inter-conversion). The (+) species enter the left boundary with a rate α_+ if that site is vacant, and leaves the right boundary with a rate β_+. The (−) species enter the right boundary with a rate α_- if that site is vacant, and leaves the left boundary with a rate β_- (Fig. 5.1).

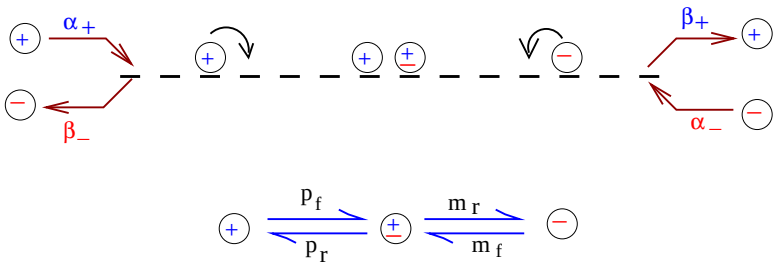

Figure 5.1: The 4-species model : The (+) hops to the right with rate 1, if the site is vacant. It enters the left boundary with rate α_+ and leaves the right boundary with rate β_+. The (−) hops to the right with rate 1, if the site is vacant. It enters the right boundary with rate α_- and leaves the left boundary with rate β_-. The (+) can convert reversibly to (±) with rates as shown. Similarly (−) can reversibly convert to (±). The (±) does not hop on the lattice.

5.2.1 Dynamic rules

We consider a 1-d lattice with N sites with sites labelled $i = 0, \ldots, N-1$, with lattice spacing $\epsilon = L/N$, where L is the total length of the lattice. The sites $i = 0$ and $i = N-1$ define the left and the right boundary respectively. The microscopic state of the system is characterized in terms of occupation numbers, n_i^+, n_i^-, $n_i^\pm$, n_i^0 of (+), (−), (±), (0) particles respectively, which takes values 0 or 1. The total occupation at each site obey the conservation law, $n_i^+ + n_i^- + n_i^\pm + n_i^0 = 1$, so that the occupation number of a vacancy, n_i^0 is fixed once the occupancy of the various types of particle is given.

We reiterate the dynamical rules:

1. For the sites $i = 0, \ldots, N-2$, (+) can hop to the neighbouring site at $i+1$, if the site is occupied by a vacancy (i.e., not occupied by (+), (−) or (±)) with a rate, 1.

2. At site $i = 0$, (+) can enter the lattice with rate, α_+, if the site is occupied by a vacancy. At site $i = N-1$, (+) leaves the lattice with rate, β_+.

3. For the sites $i = 1, \ldots, N-1$, (−) can hop to the neighbouring site at $i-1$ if the site is occupied by a vacancy (i.e., not occupied by (+), (−) or (±)) with a rate, 1.

4. At site $i = N-1$, (−) can enter the lattice with rate α_-, if the site is occupied by a vacancy. At the site $i = 0$, (−) leaves the lattice with rate β_-.

5. At each site i , (+) can transform reversibly to (±) with a forward rate p_f, the reverse rate of transformation from (±) to (+) being p_r. Similarly, at each site i , the (−) particle can transform reversibly to (±) with a forward rate m_f, the reverse rate of transformation from (±) to (−) being m_r. The rates of transformation are taken to be uniform throughout the lattice.

5.2.2 Equations of motion

We begin by writing down the equations of motion for the occupation number of the three different species in the bulk,

$$\begin{aligned}
\frac{dn_i^+}{dt} &= n^+_{i-1}(1 - n_i^+ - n_i^{\pm} - n_i^-) - n_i^+(1 - n^+_{i+1} - n^{\pm}_{i+1} - n^-_{i+1}) - p_f n_i^+ + p_r n_i^{\pm} \\
\frac{dn_i^{\pm}}{dt} &= p_f n_i^+ + m_f n_i^- - p_r n_i^{\pm} - m_r n_i^{\pm} \\
\frac{dn_i^-}{dt} &= n^-_{i+1}(1 - n_i^+ - n_i^{\pm} - n_i^-) - n_i^-(1 - n^+_{i-1} - n^{\pm}_{i-1} - n^-_{i-1}) - m_f n_i^- + m_r n_i^{\pm}
\end{aligned} \tag{5.1}$$

The terms on the right hand side of equation (5.1) have their usual interpretation of gain and loss terms at each site i, arising from translation and inter-conversion.
For the boundary at i = 0,

$$\begin{aligned}
\frac{dn_0^+}{dt} &= \alpha_+(1 - n_0^+ - n_0^{\pm} - n_0^-) - n_0^+(1 - n^+_1 - n_1^{\pm} - n_1^-) - p_f n_0^+ + p_r n_0^{\pm} \\
\frac{dn_0^-}{dt} &= n^-_1(1 - n_0^+ - n_0^{\pm} - n_0^-) - \beta_- n_0^- - m_f n_0^- + m_r n_0^{\pm}
\end{aligned} \tag{5.2}$$

For the boundary at i = N - 1,

$$\begin{aligned}
\frac{dn^-_{N-1}}{dt} &= \alpha_-(1 - n^+_{N-1} - n^\pm_{N-1} - n^-_{N-1}) - n^+_{N-1}(1 - n^+_{N-2} - n^\pm_{N-2} - n^-_{N-2}) \\
&\quad - m_f n^+_{N-1} + m_r n^\pm_{N-1} \\
\frac{dn^+_{N-1}}{dt} &= n^+_{N-2}(1 - n^+_{N-1} - n^\pm_{N-1} - n^-_{N-1}) - \beta_+ n^+_{N-1} - p_f n^-_{N-1} + p_r n^\pm_{N-1}
\end{aligned} \tag{5.3}$$

If one averages the occupation number of each species over the events that may occur between t and $t + dt$ and over all histories up to time t, then the corresponding equations of motion for the expectation value of the occupation numbers are given by,

$$\begin{aligned}
\frac{d\langle n^+_i\rangle}{dt} &= \langle n^+_{i-1}(1 - n^+_i - n^\pm_i - n^-_i)\rangle - \langle n^+_i(1 - n^+_{i+1} - n^\pm_{i+1} - n^-_{i+1})\rangle \\
&\quad - p_f\langle n^+_i\rangle + p_r\langle n^\pm_i\rangle \\
\frac{d\langle n^\pm_i\rangle}{dt} &= p_f\langle n^+_i\rangle + m_f\langle n^-_i\rangle - p_r\langle n^\pm_i\rangle - m_r\langle n^\pm_i\rangle \\
\frac{d\langle n^-_i\rangle}{dt} &= \langle n^-_{i+1}(1 - n^+_i - n^\pm_i - n^-_i)\rangle - \langle n^-_i(1 - n^+_{i-1} - n^\pm_{i-1} - n^-_{i-1})\rangle \\
&\quad - m_f\langle n^-_i\rangle + m_r\langle n^\pm_i\rangle
\end{aligned}$$

For the boundary at i = 0,

$$\begin{aligned}
\frac{d\langle n^+_0\rangle}{dt} &= \alpha_+\langle (1 - n^+_0 - n^\pm_0 - n^-_0)\rangle - \langle n^+_0(1 - n^+_1 - n^\pm_1 - n^-_1)\rangle \\
&\quad - p_f\langle n^+_0\rangle + p_r\langle n^\pm_0\rangle \\
\frac{d\langle n^-_0\rangle}{dt} &= \langle n^-_1(1 - n^+_0 - n^\pm_0 - n^-_0)\rangle - \beta_-\langle n^-_0\rangle - m_f\langle n^-_0\rangle + m_r\langle n^\pm_0\rangle
\end{aligned}$$

For the boundary at i = N - 1,

$$\begin{aligned}
\frac{d\langle n^-_{N-1}\rangle}{dt} &= \alpha_-\langle (1 - n^+_{N-1} - n^\pm_{N-1} - n^-_{N-1})\rangle - \langle n^+_{N-1}(1 - n^+_{N-2} - n^\pm_{N-2} - n^-_{N-2})\rangle \\
&\quad - m_f\langle n^+_{N-1}\rangle + m_r\langle n^\pm_{N-1}\rangle \\
\frac{d\langle n^+_{N-1}\rangle}{dt} &= \langle n^+_{N-2}(1 - n^+_{N-1} - n^\pm_{N-1} - n^-_{N-1})\rangle - \beta_+\langle n^+_{N-1}\rangle - p_f\langle n^-_{N-1}\rangle + p_r\langle n^\pm_{N-1}\rangle
\end{aligned}$$

The above set of equations are exact and in principle, the steady states or the time evolution of the expectation values can be determined from them. However to determine the

expectation value of any quantity requires the knowledge of all higher order correlations which makes it intractable analytically [7]. In specific cases like TASEP, this moment hierarchy can be handled exactly using matrix method approach [21, 22] owing to special conservation laws. In situations where the fluctuations of the number densities are smaller than mean density, a mean field approach works remarkably well [7, 15]. A case in point is the TASEP model, where the mean field theory is exact in the bulk, and correctly predicts the phase diagram [15]. In the following section we consider a specific regime of the parameter space of our model, for which we develop the mean-field theory.

5.3 Steady state for 'fast' inter-conversion rates

We analyse the dynamics when $p_f, p_r, m_f, m_r \gg 1, \alpha_\pm, \beta_\pm$, corresponding to the situation when the inter-conversion rates between $(+)$, $(-)$, $(\pm)$ are much faster than the hopping rate or the entry and exit rate of particles on the lattice. In section 5.5, we will comment on this limit in the context of motor driven vesicular transport on microtubule. In this limit, at each site i, the expectation value or the density of each type of particle is equilibrated with respect to the densities of the other type of particles at that particular site. In other words,

$$\begin{aligned} p_f\langle n_i^+\rangle &= p_r\langle n_i{}^\pm\rangle \\ m_f\langle n_i^-\rangle &= m_r\langle n_i{}^\pm\rangle \end{aligned} \tag{5.4}$$

The equations for steady state in the bulk are now given by,

$$\langle n^+_{i-1}(1-n_i^+-n_i{}^\pm-n_i^-)\rangle = \langle n_i^+(1-n^+_{i+1}-n^{\pm}_{i+1}-n^-_{i+1})\rangle \tag{5.5}$$

$$\langle n^-_{i+1}(1-n_i^+-n_i{}^\pm-n_i^-)\rangle = \langle n_i^-(1-n^+_{i-1}-n^{\pm}_{i-1}-n^-_{i-1})\rangle \tag{5.6}$$

5.4 Mean-field and continuum limit

Defining $\rho_i^+ \equiv n_i^+$, $\rho_i^- \equiv n_i^-$ and $\rho_i^\pm \equiv n_i^\pm$, the mean field approximation amounts to factorizing all the two-point correlators arising out of the different combinations of $n_i^+, n_i^-, n_i^\pm$ as a product of their averages,

$$\langle n_i n_{i+1}\rangle = \rho_i\rho_{i+1} \tag{5.7}$$

We now go over to a continuum description. We normalize the total length of the lattice, L, to 1 and let $N \to \infty$, so that the lattice spacing $\epsilon = \frac{L}{N} \to 0$ in the thermodynamic limit.

We express the steady states in terms of individual densities of (+), (−), (±). The rescaled position variables are defined as $x = \frac{i}{N-1}$, so that $0 \leq x \leq 1$.

Transformations from discrete to continuum variables are given by,

$$\begin{aligned} \langle\, n_i^+ \,\rangle &= \rho_+(x,t) \\ \langle\, n_{i+1}^+ \,\rangle &= \rho_+(x,t) + \epsilon\rho_+^{'}(x,t) + \frac{\epsilon^2}{2}\rho_+^{''}(x,t) \\ \langle\, n_{i-1}^+ \,\rangle &= \rho_+(x,t) - \epsilon\rho_+^{'}(x,t) + \frac{\epsilon^2}{2}\rho_+^{''}(x,t) \end{aligned} \tag{5.8}$$

Similarly one can relate the other expectation values, $\langle\, n_i^- \,\rangle$ and $\langle\, n_i^\pm \,\rangle$ to the corresponding continuum densities. The densities of the individual species at the steady state, for 'fast' inter-conversion rates are themselves related with each other by equation (5.4),

$$\begin{aligned} \rho_\pm(x) &= K_+\rho_+ \\ \rho_\pm(x) &= K_-\rho_- \end{aligned} \tag{5.9}$$

where $K_+ = p_f/p_r$ and $K_- = m_f/m_r$ are the equilibrium rate constants of the transformation $+ \rightleftharpoons \pm$ and $- \rightleftharpoons \pm$ respectively.

5.4.1 Equations of motion in bulk

The equation of motion for ρ_+ is obtained from equation (5.5) by first invoking the mean-field assumption, equation (5.7), and then using equation (5.8) to express everything in term of the density variables. Subsequently, we use equation (5.9) to eliminate ρ_- and $\rho_\pm$ in favour of ρ_+,

$$\frac{\partial\rho_+}{\partial t} = -\frac{\partial}{\partial x}\left[-\frac{\epsilon}{2}\frac{\partial\rho_+}{\partial x} + \rho_+(1 - W_+\rho_+)\right] \tag{5.10}$$

where,

$$W_+ = 1 + K_+ + \frac{K_+}{K_-} \tag{5.11}$$

Similarly the equation of motion for ρ_- is

$$\frac{\partial\rho_-}{\partial t} = -\frac{\partial}{\partial x}\left[-\frac{\epsilon}{2}\frac{\partial\rho_-}{\partial x} - \rho_-(1 - W_-\rho_-)\right] \tag{5.12}$$

where,

$$W_- = 1 + K_- + \frac{K_-}{K_+} \tag{5.13}$$

Equations (5.10) and (5.12) are the usual continuity equations with,

$$J_+ = -\frac{\epsilon}{2}\frac{\partial \rho_+}{\partial x} + \rho_+(1 - W_+\rho_+) \tag{5.14}$$

$$J_- = -\frac{\epsilon}{2}\frac{\partial \rho_-}{\partial x} - \rho_-(1 - W_-\rho_-) \tag{5.15}$$

J_+ and J_- have the interpretation of being the currents of the (+) and (−) species respectively.

5.4.2 Steady state

The steady state is simply given by

$$-\frac{d}{dx}\left[-\frac{\epsilon}{2}\frac{d\rho_+}{dx} + \rho_+(1 - W_+\rho_+)\right] = 0 \tag{5.16}$$

$$-\frac{d}{dx}\left[-\frac{\epsilon}{2}\frac{d\rho_-}{dx} + \rho_-(1 - W_-\rho_-)\right] = 0 \tag{5.17}$$

In the thermodynamic limit, $\epsilon \to 0$ this implies that the currents J_+, J_- are constant in the bulk with no spatial variation. Further they are related to each other by,

$$J_+ = -\frac{K_-}{K_+}J_- \tag{5.18}$$

5.4.3 Matching conditions at the boundaries

So far we have said nothing about the input and output currents, $\alpha_\pm, \beta_\pm$. They now appear as the boundary condition to be satisfied by equations (5.16) and (5.17). The natural boundary condition is to equate the bulk current (comprising of currents due to (+) and (−)), evaluated at the boundary to the total current due to input and output rate of (+) and (−) at the boundary. Thus at the left boundary, x = 0,

$$\alpha_+ \left[1 - W_+\rho_+(0)\right] - \beta_-\rho_-(0) = \rho_+(0)\left[1 - W_+\rho_+(0)\right] - \rho_-(0)\left[1 - W_-\rho_-(0)\right] \tag{5.19}$$

Using the above equation and denoting $\rho_+(0) = \rho^+_{LD}$ we get the density consistent with left boundary condition as,

$$\rho^+_{LD} = \frac{M - \left[M^2 - 4\alpha_+ W_+\left(1 - \frac{K_+}{K_-}\right)\right]^{\frac{1}{2}}}{2W_+\left(1 - \frac{K_+}{K_-}\right)} \tag{5.20}$$

where,

$$M = \alpha_+ W_+ + \beta_- \frac{K_+}{K_-} + 1 - \frac{K_+}{K_-} \tag{5.21}$$

The corresponding expression of current consistent with this boundary condition is given by,

$$J^+_{LD} = \rho^+_{LD}(1 - W_+\rho^+_{LD}) \tag{5.22}$$

Similarly at the right boundary, x = 1,

$$-\alpha_-[1 - W_-\rho_-(1)] + \beta_+\rho_+(1) = \rho_+(1)[1 - W_+\rho_+(1)] - \rho_-(1)[1 - W_-\rho_-(1)] \tag{5.23}$$

Denoting $\rho_+(1) = \rho^+_{HD}$, we get the density consistent with right boundary condition as,

$$\rho^+_{HD} = \frac{P + \left[P^2 + 4\alpha_- W_+\left(1 - \frac{K_+}{K_-}\right)\right]^{\frac{1}{2}}}{2W_+\left(1 - \frac{K_+}{K_-}\right)} \tag{5.24}$$

where,

$$P = -\alpha_- W_+ - \beta_+ + 1 - \frac{K_+}{K_-} \tag{5.25}$$

The corresponding expression for current is given by,

$$J^+_{HD} = \rho^+_{HD}(1 - W_+\rho^+_{HD}) \tag{5.26}$$

5.5 Phase diagram and domain wall analysis

5.5.1 The phases

If we look at the steady state condition discussed in the previous section, we find that in the limit of $\epsilon \to 0$, both the boundary conditions cannot be satisfied simultaneously. Therefore either the steady state solution satisfies the boundary condition at the left (x = 0) or it satisfies the boundary condition at the right (x = 1) and both of these correspond to the two possible stationary states and correspondingly two different phases.

In addition, there is one more phase, the maximal current phase. If we go back to the original expression of current (equation 5.14), then we see that there is an upper bound on the maximum current J^{max}_+, that the lattice can sustain. Note that the current of (+) species on the lattice is simply $\rho_+[1 - W_+\rho_+]$, so that

$$J^{max}_+ = Max\left[\rho_+(1 - W_+\rho_+)\right] \tag{5.27}$$

This suggests there is another phase, corresponding to the maximum value of current, obtained by maximizing expression for current given in equation (5.27). The three different phases are:

1. **Low density phase** corresponding to the stationary state determined by the left boundary condition. In this phase, the density and the current of (+) species is given by equations (5.20) and (5.22). The density of $(-), (\pm)$ are then fixed by equation (5.9). The current for $(-)$ can be evaluated using the expression in equation (5.17).

2. **High density phase** corresponds to the stationary state determined by the boundary conditions at the right. In this phase the density and current of the (+) particles are given by equations (5.24) and (5.26), and as in the case of the low density phase the density and currents of (-) and density of $(\pm)$ can be determined.

3. **Maximal current phase**, corresponds to stationary state determined by maximizing the expression for the current. Thus the expression for the density and current is given by,

$$\begin{aligned} \rho_+ &= \frac{1}{2W_+} \\ J_+ &= \frac{1}{4W_+} \end{aligned} \tag{5.28}$$

Plots of the steady state value of densities and current obtained by Monte-Carlo simulations for all the three phases are shown in Figs (5.3 - 5.5). They show a good match with the mean-field values of the density and current in the bulk.

5.5.2 Selection of phases: domain wall dynamics

In order to construct the whole phase diagram, we need to know the criterion for selection of a particular phase. A physical way of understanding the phase selection criterion is to analyse it terms of *domain wall dynamics*, as we elaborate below. We will briefly review the domain wall picture for TASEP [15], as we are subsequently going to use this approach to determine the phase boundaries in our minimal model.

In TASEP, particles enter an N-site lattice from the left with a rate α provided the first site is empty. Within the lattice, the particle hops to the next left with rate 1 provided that this site is empty and it leaves the last site with a rate β. These choice of rates corresponds to coupling the system to reservoirs with constant densities, α and $1-\beta$ respectively. The three

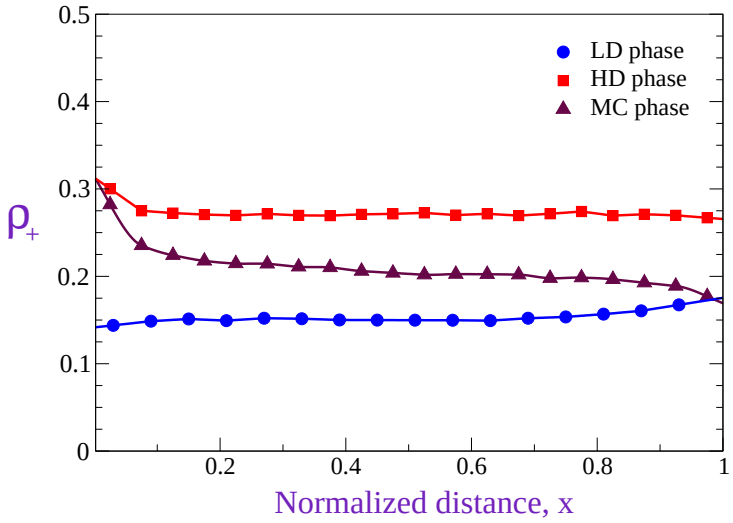

Figure 5.2: Steady state spatial distribution of density for (+) species obtained by Monte-Carlo simulation illustrating the different possible phases, ($\alpha_- = 0.2$, $\beta_- = 0.2, K_+ = 1, K_- = 2$) . (A) LD phase ($\alpha_+ = 0.1, \beta_+ = 0.9$), $\rho_+^{MF} = 0.15$. (B) HD phase ($\alpha_+ = 0.6$, $\beta_+ = 0.4$), $\rho_+^{MF} = 0.27$. (C) MC phase ($\alpha_+ = 0.6, \beta_+ = 0.9$), $\rho_+^{MF} = 0.2$.

possible steady states correspond to the low density phase (LD), high density (HD) and the maximal current (MC) phase, as shown in Fig. 5.2. When the particles are supplied at the left end with a rate $\alpha > \beta$, and removed slowly at the right end , $\beta < \frac{1}{2}$, then the result is an HD phase, for which particle extraction is the limiting process. When the particles are removed at the right end with a rate $\beta > \alpha$, and supplied slowly at the left, $\alpha < \frac{1}{2}$, the result is an LD phase, for which particle supply is the limiting process. When the particles are supplied and removed fast, $\alpha > \frac{1}{2}, \beta > \frac{1}{2}$, then there is a phase transition into a MD phase for which transport is limited by the bulk and current takes its maximum value of $\frac{1}{4}$. There is a first order transition line separating the LD and HD phase. The density changes discontinuously across this boundary. However the density changes continuously across the LD-MC phase and the HD-MC phase boundary.

To gain physical insight of the phases and their stability in TASEP, it is useful to consider the following example :

Let us assume that α and β are very small ($\alpha N \ll 1, \beta N \ll 1$) and that the initial distribution of particles is far from the true stationary state. At late times, there will be a low density region at the left and a high density region at the right, as the particles will get stuck. This is

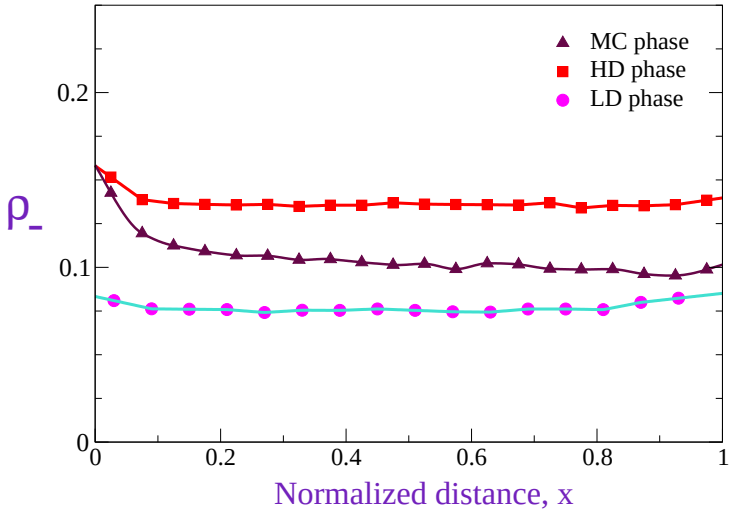

Figure 5.3: Steady state spatial distribution of density for (-) species obtained by Monte-Carlo simulation for the same parameter values as in Fig. 5.2. The corresponding densities obtained by mean field: (A) LD phase: $\rho_-^{MF} = 0.075$. (B) HD phase: $\rho_-^{MF} = 0.135$. (C) MC phase: $\rho_-^{MF} = 0.1$.

schematically represented as (00001111) with a domain wall separating the low density (0) and high density (1) phases. The subsequent time evolution can be interpreted in terms of the motion of this domain wall.

When a particle exits the right boundary, then the remaining particles would rearrange themselves such that the domain wall shifts by one lattice unit to the right. Similarly whenever a particle enters the right boundary, then the domain wall would shift one unit to the left. So essentially the domain wall does a biased random walk, with a drift velocity $V_d = \beta - \alpha$ and a diffusion constant $D = \frac{\alpha+\beta}{2}$. As a result, there exist three possible scenarios. If $\alpha < \beta$, then the domain wall drifts to the right and will eventually reach the end of the system, so that the system is in a low density stationary state. For $\alpha > \beta$, the domain wall will eventually drift to the left boundary, resulting in the high density phase. For $\alpha = \beta$, the domain wall fluctuates with no drift velocity and its root mean square velocity increases with time as $\sqrt{Dt}$. As a consequence, one would expect a linearly increasing density profile, corresponding to the phase boundary between the LD and HD phase. Next, let us consider the case when $\alpha > \frac{1}{2}$ and β is small. We start from an empty lattice and after a while, but before the true stationary state is established, the system would consist of two linear segments. On

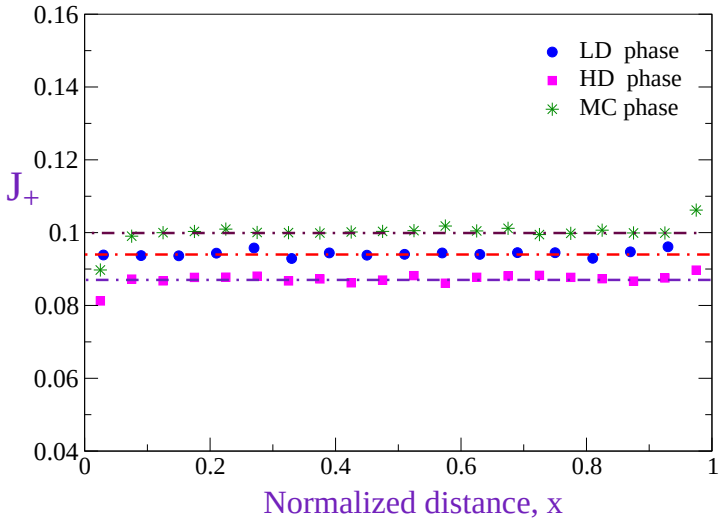

Figure 5.4: Steady state spatial distribution of current of (+) species obtained by Monte-Carlo simulation for the same parameter values as in Fig. 5.2. The corresponding current obtained by mean field: (A) LD phase: $J_+^{MF} = 0.094$. (B) HD phase: $J_+^{MF} = 0.087$. (C) MC phase: $J_+^{MF} = 0.1$.

the left would be a region closely resembling the maximal current phase (m), due to the high entry rate of particles. On the right end there will be a phase resembling the high density phase (1), since the transport is limited by the exit rate, β. This is schematically represented by (mmmm1111). So again there is a domain wall and the final steady state is determined by its drift velocity. Even for the more general case, where the entry and exit rates are not small, this picture of the domain wall holds good. Essentially, the domain wall should be understood as a region separating two distinct stationary states. Consider a region in the bulk separating two different phases, say the high density phase and the low density phase. Note that the local particle density in the bulk obeys the continuity equation, $\frac{\partial \rho_+}{\partial t} + \frac{\partial j_+}{\partial x} = 0$. Such an equation will admit a travelling wave solution of the form $\rho_+(x - V_d t)$. With this form of solution and integrating the continuity equation between $-\infty$ and $+\infty$, we get

$$V_d = \frac{J_+^R - J_+^L}{\rho_+^R - \rho_+^L}, \tag{5.29}$$

where J_+^R, ρ_+^R are the density and current to the right of the domain wall and J_+^L, ρ_+^L are the density and current to the left of the domain wall. V_d has the interpretation of the drift ve-

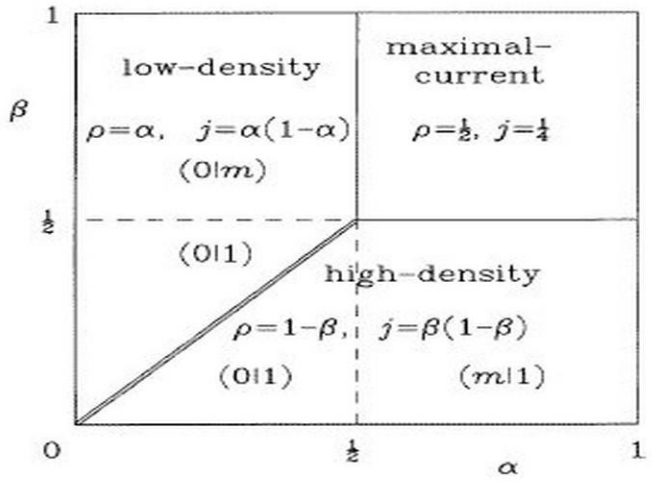

Figure 5.5: The phase diagram from TASEP with stationary values of the particle density ρ, current j, and allowed types of domain walls: LD/HD (0|1), MC/HD (m|1) and LD/MC ($0/m$) [15].

locity of the domain wall. For a LD-HD phase boundary in the bulk, if $V_d > 0$, the domain wall will drift to the right boundary. Thus at late times, the steady state will be a low density phase. Similarly if $V_d < 0$, the domain wall will drift towards the left boundary and the bulk density profile will be a high density phase. $V_d = 0$ defines the phase co-existence curve of the two phases.

Moving across the phase boundary between the low density and high density phases results in a discontinuous (first order) change of density, as we will see in a subsequent analysis. Similarly, the phase boundary between a LD or HD and the maximal current phase (MC) is associated with a continuous phase transition, where the density changes continuously.

5.5.3 Domain wall boundaries

We now apply the domain wall analysis to our 4-species model. As discussed earlier in section (5.3), as a consequence of 'fast' inter-conversion, the density of any one species, fixes the densities of the other species. Thus we can look at the phase of any one of the species and immediately fix the nature of phase for the other species, so that there are only three kind of phases which are possible, as was discussed in section (5.5.1). Thus we can analyse the phase and phase boundaries for one of the species and determine the rest. We can have three different kinds of domain walls:

1. LD-HD domain wall schematically represented as (0 | 1)
2. LD-MC domain wall schematically represented as (0 | m)
3. MC-HD domain wall schematically represented as (m | 1)

From equation (5.29), the expression for the domain wall velocity is given by,

$$V_d = 1 - \frac{\rho_+^L + \rho_+^R}{W_+} \tag{5.30}$$

where ρ_+^L, ρ_+^R are the density of (+) particles to the left and right of the domain wall respectively. The condition $V_d = 0$ gives the equation of the phase boundary.

To obtain the LD-MC phase boundary, we study the velocity of the LD-MC domain wall. Taking $\rho_R^+ = \rho_{MC}^+$ and $\rho_L^+ = \rho_{LD}^+$, and putting $V_d = 0$ in equation (5.30), we obtain the equation of the phase boundary as,

$$\alpha_+ = \frac{1}{2\,W_+}\left(2\beta_- \frac{K_+}{K_-} + 1 - \frac{K_+}{K_-}\right) \tag{5.31}$$

Thus in the $(\alpha_+ - \beta_+)$ plane, the phase boundary is a straight line parallel to α_+ axis.

To obtain the MC-HD phase boundary, we study the velocity of the MC-HD domain wall. Taking $\rho_L^+ = \rho_{MC}^+$ and $\rho_R^+ = \rho_{HD}^+$, and putting $V_d = 0$ in equation (5.30), we obtain the equation of the phase boundary as,

$$\beta_+ = \frac{1}{2}\left(1 + 2\alpha_- W_+ - \frac{K_+}{K_-}\right) \tag{5.32}$$

So in the $(\alpha_+ - \beta_+)$, plane the phase boundary is a straight line parallel to β_+ axis.

We see that beyond a critical value of α_- , the exit rate of (−) species, $\beta_+ > 1$, implying that the maximal current phase does not occur in this range of entry and exit rates. Thus the high density phase and the low density phase are the only two phases which can occur in such a situation.

To obtain the LD-HD phase boundary, we study the velocity of the LD-HD domain wall. Taking $\rho_R^+ = \rho_{HD}^+$ and $\rho_L^+ = \rho_{LD}^+$, the equation of the phase boundary has a cumbersome form, $\alpha_+ = f(\beta_+, K_+, K_-, \beta_-, \alpha_-)$, which can be easily evaluated numerically. Fig. 5.6 and Fig. 5.7 show the phase boundary curve between high density and low density region, evaluated numerically.

What is of interest, is the fact that the shape of the domain wall boundary and the location is crucially dependent on the rate constants and the entry and exit rates of (−) particles. For certain values of rate constants, the maximal current phase does not exist in the physically realizable regime of entry and exit rates of particles (Fig. 5.7).

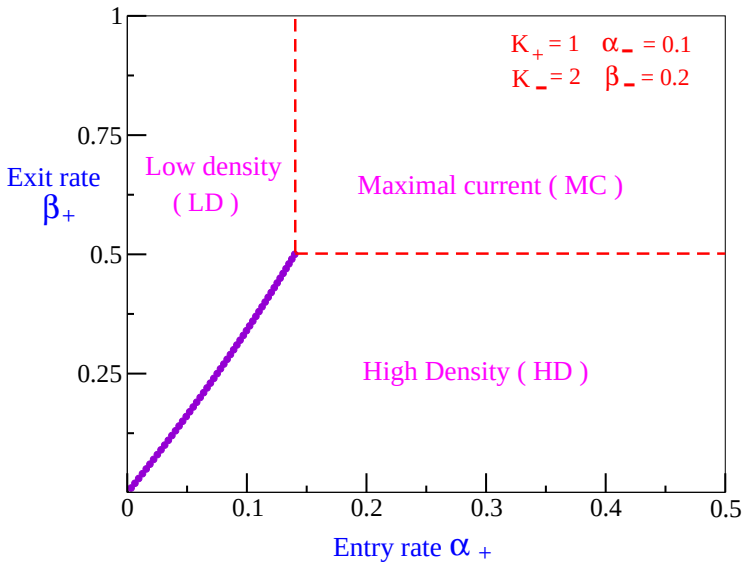

Figure 5.6: Section of the phase diagram for 4-species model, for $K_+ = 1, K_- = 2, \alpha_- = 0.1, \beta_- = 0.2$. Note that unlike the phase diagram for TASEP the first-order phase boundary curve separating the LD and HD phase is not a straight line.

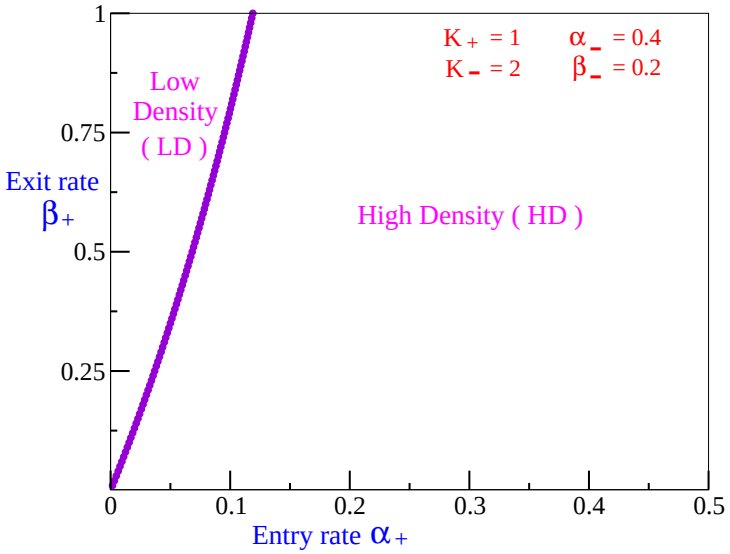

Figure 5.7: Section of the phase diagram for 4-species model, for $K_+ = 1, K_- = 2, \alpha_- = 0.4, \beta_- = 0.2$. Notice that changing the entry rate of $(-)$ from 0.1 to 0.4 has resulted in a change in the nature of the phase diagram, such that there is no maximal current phase.

5.6 Conclusions

We have looked at a simplified minimal model for the collective transport of interacting 'particles' and determined its phases using a mean-field analysis and domain wall approach. Even though highly simplified, this minimal model does illustrate the effects of the particle interaction (via simple excluded volume effects) and finite boundaries on the bulk profile of the phases. It also highlights the effects of processivity, the (un)binding rates of the motors, in determining the bulk phase.

We comment on the 'fast' inter-conversion limit. To get a feel for its validity, let us look at the typical rates encountered in the cellular context. We will look at the two examples of bidirectional transport we had discussed in Chapter 4.

1. Transport of melanosomes: Recall that the (un)binding rates of kinesin are $\sim 1/sec$ [23, 24], while the typical cargo velocities are $\sim 1\mu m/s$ [25]. The typical length of the microtubule track is $\sim 50\mu m$ [25]. Clearly 'fast' inter-conversion limit implies that there are large number of inter-conversion events, before an hopping event occurs. An appropriate choice of the coarse-grained lattice spacing, ϵ, specifies the effective step length needed to satisfy this limit. With the numbers quoted above, the scale $\epsilon \gg 1\mu m$, which is a fair fraction of the total length of the microtubule track. This would make our analysis in section (5.3) inapplicable.

2. Transport of mitochondria on axons : If we look at microtubule based axonal transport of mitochondria, then velocities of mitochondria is measured to be $\sim 0.25\mu m/s$ [1]. The typical length of the axon is $\sim 150\mu m$ [1]. Taking a lattice spacing of 1.5 μm, reasonably insures the criterion of fast inter-conversion. Also note that organelles are of comparable size, ensuring that there is only 1 particle per 'site'. With this value of lattice spacing, ϵ, one has ~ 100 lattice sites, so that one can reasonably describe the steady states and phases in terms of the minimal model with 'fast' inter-conversion.

In situations where this limit does not hold, a full Monte-Carlo simulation will be needed to determine the steady states and the corresponding phases.

One possible extension of the work would be to extend this model to the case when the vesicle density is not conserved, either because the motor vesicle complex is transferred from one track to another [25], or because they leave the track and diffuse through the cytoplasm, before reattachment.

Bibliography

[1] R. L. Morris and P. J. Hollenbeck, J. Cell. Sc. **104**, 917 (1993).

[2] R. Mallik and S. P. Gross, Curr. Biol. **14**, R971 (2004).

[3] N. Hirokawa, R. Sato-Yoshitake, N. Kobayashi, K. K. Pfister, G. S. Bloom and S. T. Brady, J. Cell. Biol. **114**, 295 (1991)

[4] L. T. Haimo, Trends. Cell. Biol. **5**, 165 (1995).

[5] S. Mukherji and S. M. Bhattacharjee, J. Phys. A: Math. Gen. **38**, L285 (2005).

[6] Y. Kafri, E. Levine, D. Mukamel, G. M. Schutz and R. D. Wilmann, Phys. Rev. E. **68**, 035101(R) (2003).

[7] V. Privman (ed.) in *Nonequilibrium Statistical Mechanics in One Dimension* (Cambridge University Press, Cambridge, 1997).

[8] D. E. Wolf, M. Schreckenberg and A. Bachem (eds.) in *Traffic and Granular Flow* (World Scientific, Singapore, 1996).

[9] D. Chowdhury, L. Santen and A. Schadschneider, Phys. Rep. **329**, 199 (2000).

[10] M. Barma and R. Ramaswamy in *Non-Linearity and Breakdown in Soft Condensed Matter* (Springer, Berlin, 1993).

[11] A. Parmeggiani, T. Franosch and E. Frey, Phys. Rev. Lett. **90**, 086601 (2003).

[12] G. Tripathy and M. Barma, Phys. Rev. E. **58**, 1911 (1998).

[13] M. R. Evans and T. Hanmey, J. Phys. A: Math. Gen. **38**, R195 (2005).

[14] A. Parmeggiani, T. Franosch and E. Frey, Phys. Rev. E. **70**, 046101 (2004).

[15] A. B. Kolomeisky, G. M. Schutz, E. B. Kolomeisky and J. P. Straley, J. Phys. A **31**, 6911 (1998).

[16] V. Popkov and G. M Schutz, Europhys. Lett. **48**, 257 (1999).

[17] J. T. MacDonald, J. H. Gibbs and A. C. Pipikin, Bioploymers **6**, 1 (1968).

[18] B. Schmittmann and R. K. P. Zia in *Phase Transitions and Critical Phenomena, Vol. 17*, ed C. Domb and J. Lebowitz, (Academic, London, 1995).

[19] J. Krug, Phys. Rev. Lett. **67**, 1882 (1991).

[20] B. Derrida, E. Domany and D. Mukamel, J. Stat. Phys. **69**, 667 (1992).

[21] G. Schutz and E. Domany, J. Stat. Phys. **72**, 277 (1993).

[22] B. Derrida, M. R. Hakim, V. Pasquier, J. Phys. A: Math. Gen. **26**, 1493 (1993).

[23] S. M. Block, L. S. B Goldstein and B. J. Schnapp, Nature **348**, 348 (1990).

[24] R. D. Vale, T. Fanatsu, D. W. Pierce, L. Romberg, Y. Harada and T. Yanagida, Nature **380**, 451 (1996)

[25] V. I. Rodionov, A. J. Hope, T. M. Svitkina and G. G. Borisy , Curr. Biol. **8**, 165 (1998).

[26] M. A. Welte, Curr. Biol **14**, R525 (2004).

[27] B. Alberts et al., in *Molecular Biology of the Cell* (Garland Science, New York, 2002, 4th ed).

Synopsis

The underlying theme of this thesis is the study of mechanics and transport in cellular filaments. A variety of cellular processes involving these filaments are *active*. Indeed activity is crucial in determining the rheology and transport properties within the cell. Activity plays itself out by the interplay between chemical kinetics of protein machines and the mechanics of the filaments. In this thesis, we study theoretical models for the mechanics and transport in cellular filaments in four different contexts :

- Sequence-dependent elastic properties of DNA and its implications for DNA-protein binding.
- Shear flow stabilization and rheology of orientationally ordered *active* matter (e.g., actin-myosin, motor-microtubule complexes).
- Active bidirectional transport of vesicles on microtubules.
- Collective transport of interacting vesicles on microtubules.

While the contexts are distinct, they reaffirm our basic thesis and highlight the interplay of activity, chemistry and mechanics in cellular filaments. The models that we study, broadly, falls under the purview of non-equilibrium statistical mechanics of driven systems.

Summary of results

Sequence-dependent elastic properties of DNA and its implications for DNA-protein binding kinetics: We study the 'sequence'-distribution of thermally averaged global and local elastic properties of a DNA random heteropolymer of a fixed length N, within a simple elastic, worm-like chain (WLC) model. Using a mapping to the disordered Heisenberg chain, we arrive at a number of qualitative results on the form of the distribution function of the thermally averaged end-to-end distance $\langle R^2 \rangle$, and its moments. For long, $N \to \infty$, chains, this distribution is a gaussian; for shorter chains, there is a crossover to an exponential distribution, with the most probable end-to-end distance deviating significantly from the mean. Further, the distribution of local quantities related to the thermally averaged tangent-tangent

correlator are typically broad, even in the thermodynamic limit, *i.e., they do not self average*. We argue that this scale dependent 'sequence' sensitivity should have important biological implications, specifically for the binding of proteins to DNA — we present a simple model calculation of the binding/unbinding kinetics of DNA-binding proteins, with numerical estimates for the human DNA-repair enzyme HOGG1.

Shear flow stabilization and rheology of orientationally ordered active matter: We study the effects of externally applied shear flow on a model of suspensions of motors and filaments, via the equations of active hydrodynamics [PRL **89** (2002) 058101; **92** (2004) 118101]. In the absence of shear, the orientationally ordered phase of *both* polar and apolar active particles is always unstable at zero-wavenumber. We find that an imposed steady shear large enough to overcome the active stresses stabilises both apolar and moving polar phases beyond a critical *active* Peclet number defined by the ratio of the shear to active stress. We study the novel rheological behaviour of the stabilized orientationally ordered phase. Our work is relevant to *in vitro* studies of active filaments, the reorientation of endothelial cells subject to shear flow and shear-induced motility of attached cells.

Active bidirectional transport of vesicles on microtubules: We study bidirectional vesicular transport on microtubules by multiple processive motors, using a single-particle transition rate model. This model is relevant to a class of *in-vitro* experiments. We make specific qualitative and quantitative predictions of various transport properties such as distribution of the velocity of the vesicles, first passage time of unbinding of the vesicle from the microtubule, distribution of reversal times of the vesicles and average number of attached motors to the microtubule. This allows us to compute the statistics of trajectories of the vesicles, which can be compared to single particle tracking experiments in live cells. We beleive that our model can be used to study the dynamics of vesicle transport in melanophore and axonal transport of mitochondria.

Collective transport of interacting vesicles on filaments: A single-particle model of transport of vesicles on filaments is appropriate only in the limit of low concentration of vesicles, when the effects of inter-vesicle interactions can be ignored. We study a minimal 4-species model for vesicle transport, which incorporates the effects of interactions between vesicles and the effects of finite boundaries. We look at the steady state profiles of system in the limit of 'fast'interconversion among the various species. We determine the nature of the phases and the corresponding phase boundaries using continuum mean-field analysis, and find exact agreement with Monte-Carlo simulation. We analyse the phases and dynamics

using a domain wall approach. Finally, we discuss this minimal model in the context of collective transport of vesicles on microtubules.

Publications / Manuscripts

[1] "Shear flow induced isotropic to nematic transition in a suspension of active filaments", Sudipto Muhuri, Madan Rao and Sriram Ramaswamy, *cond-mat/0610025, submitted to Europhys. Lett*.

[2] "Sequence - dependent elasticity and local stiffness of a DNA heteropolymer", Sudipto Muhuri and Madan Rao, *to be submitted*.

Prof. Madan Rao
Theoretical Physics Group
Raman Research Institute
Bangalore, INDIA

Sudipto Muhuri
Theoretical Physics group
Raman Research Institute
Bangalore, INDIA